Available online at www.sciencedirect.com
ScienceDirect
Cement and Concrete Research 38 (2008) 649–659
Cement and Concrete Research

Evolution of penetration resistance in fresh concrete

Alvaro García *, Daniel Castro-Fresno, Juan Antonio Polanco

Escuela de Caminos, Canales y Puertos de Santander, Departamento de Transportes, avda. los Castros s/n. 39005, Universidad de Cantabria, Santander, Spain

Received 6 June 2006; accepted 29 October 2007

Abstract

The objective of this research was to examine the setting of concrete through its penetration resistance; an experimental device, especially developed for this purpose was used, which consists of a system that lets a sphere fall on concrete from a certain height and then measures the depth of the crater. Forty-five samples were made with four different types of cement varying its quantity, water–cement ratio, at ambient temperature and humidity. A semiempirical model which explains the penetration resistance evolution in fresh concrete was proposed and experimentally demonstrated. The results are compared with the consolidation curves for soils represented by the logarithmic method. The proposed setting time was defined as the elapsed time between the placement of the concrete and the time when the depth of the crater is 18% of the initial one.

Keywords: Fresh concrete (A); Adsorption (C); Kinetics (A); Secondary consolidation; Modeling (E)

1. Introduction

Concrete suffers an important transformation from when it is mixed until the initial setting time. Traditionally, fresh concrete has been considered a viscoelastic material [1,2]. However, from another point of view, it may be described as an assembly of particles made up of water and cement joined by the friction among them and by the van der Waals forces [3], among which a series of chemical processes take place that makes the concrete harden.

The hardening process of concrete in its first stages is excellently described by means of the percolation theory [4]. Hammersley [5] was the first to study this in the 1950s. The percolation theory deals with the components connectivity of a system, where its disorder is defined as a variation in its connectivity level [6]. According to this theory, for a given system in three dimensions, the critical percolation degree is 16% of porosity [5,7]. This value is called "depercolation threshold", and in concrete coincides with the initial setting time, or the moment when the first solid paths are formed in the hardening paste. Therefore, the setting of concrete will depend, not only on the penetration resistance in the fresh concrete at a given time, but also on those factors which affect the connectivity level between particles and voids such as its consistency. The penetration resistance evolution in fresh concrete was traditionally considered as a way to know the initial and final setting times by mechanical means, depending on the applied force and the system geometry.

The Vicat needle [8] is the most widely used method to find the set of cement paste. In a sample of cement made with enough water to have what is called "normal consistency", initial and final set are measured from the penetration of an 1 mm diameter needle with a length of 50 mm and a plunger weight of 300 g. Another alternative system is to measure the heat developed on concrete during the first hours [9], defining the initial setting time when 12.5 kJ of heat are liberated per cement kg.

The set of concrete and mortar can be checked with the Proctor needles, described in the ASTM C403 and first studied by Tuthill and Cordon [10]. In this method, based on the same principle as the Vicat one, the initial setting time is defined as the lapsed time from the initial contact between the cement and the water, until the penetration resistance of mortar extracted from

* Corresponding author.
E-mail address: alvarogarcia007@hotmail.com (A. García).

0008-8846/$ - see front matter © 2007 Elsevier Ltd. All rights reserved.
doi:10.1016/j.cemconres.2007.10.005

concrete using a sieve is 3.5 MPa and 27.6 MPa for the initial and final setting time respectively [11].

However, none of these methods provides precise information of the period of time before initial setting. By means of the Vicat needle, this time cannot be measured, while using the Proctor needles for concrete the first minutes in the penetration resistance curve are almost ignored, although they are essential for the microstructure development of cement paste and concrete. Starting from the percolation theory, any comparison made between the results obtained of cement paste through a Vicat needle with a mortar tested through the Proctor method would be impossible unless both samples have the same initial consistency, water–cement ratio and cement.

Schindler [12], starting from the concept of "critical hydration degree", first defined by Byfors [13] identified the hydration degrees at initial and final setting from Proctor tests as a constant multiplied by the water–cement ratio. This was based on the idea that a higher water–cement ratio implied a bigger distance between the cement particles, so that a higher hydration degree would be required to obtain resistance. At first glance, the concept seems logical from the percolation theory point of view. Nevertheless, in the formation of the first solid paths in concrete, the most important parameter is the proximity between all the particles, which is a variable influenced by a high number of factors, from the vibration of concrete to the aggregate grading.

In this paper, a semiempirical model that explains the penetration resistance evolution in fresh concrete is proposed. As a hypothesis, fresh concrete has been considered to behave as a non-saturated soil made of water, air, cement particles and aggregates, with a yield stress given by the friction between them, van der Waals forces and chemical reactions, whose stiffness varies with time due to cement hydration. A theoretical equation for penetration resistance is proposed and experimentally checked.

2. Methodology and materials

2.1. Test method

The device used to measure the penetration resistance in fresh concrete consists of a frame supporting a PVC pipe, which placed on a mold of 60 × 60 × 15 cm lets a sphere fall onto the concrete from a certain height causing an impact (Fig. 1); then, the depth of the crater is measured. Spheres of different diameters and mass were used, although as will be explained, this is irrelevant for the evolution of the model of penetration resistance. The maximum precision that could be obtained in the measurement was ± 1 mm.

2.2. Test results analysis

The configuration of forces acting on a sphere moving into fresh concrete will change in a very complex fashion as it moves through the medium [14]. A sphere with mass (m) falling from rest at height (H), will perforate a crater of depth (y) and transfer the whole energy of the system to the concrete. So, when a differential increase of stress ($\Delta\sigma$) is applied, an increase of deformation ($\Delta\varepsilon$) will take place, which will be partly elastic and partly plastic. The work done in deformation will be:

$$\Delta W = \sigma_{ij} \cdot \Delta\varepsilon_{ij}. \quad (1)$$

A simplified way to consider the total stress applied by the medium on the projectile, is to divide the whole potential energy by the concrete volume (V) displaced in the penetration [15–18]:

$$m \cdot g \cdot H = \sigma \cdot V. \quad (2)$$

Therefore, σ will be the total or deviatoric stress exerted by the penetration resistance forces on the sphere, which are given by the characteristics of the element penetrating in concrete, its own weight, the Archimedes force, the viscous resistance force in the case when the concrete has not acquired enough resistances and the sliding resistance between the sphere and the medium.

de Bruyn and Walsh [19] demonstrated that the penetration depth of spheres impacting on a granular media is linearly dependent on the moment or, the sphere mass and the height from which it falls. This behavior can be explained in terms of yield stress and effective viscosity of the granular media. On the other hand, Chen and Li [20] stated that in the case of deep penetration of a non-deformable projectile, or in other words, in the case that the penetration depth (y) is greater than the projectile diameter (d) adding its nose, the adimensional penetration (y/d) of the projectile in the material, will behave linearly with regard to a non-dimensional number, called the impact function (I), hardly depending on the geometry, mass and the projectile impact speed.

There are several theories relating the soil or concrete properties and their penetration resistance, among which, the most popular is the cavities expansion theory, established by Bishop in 1945 [21]. In the case of a sphere of radius (R) penetrating in fresh concrete at a certain speed, at the point 0 (Fig. 2), a spherical cavity is created that expands up to a radius R,

Fig. 1. Test device view.

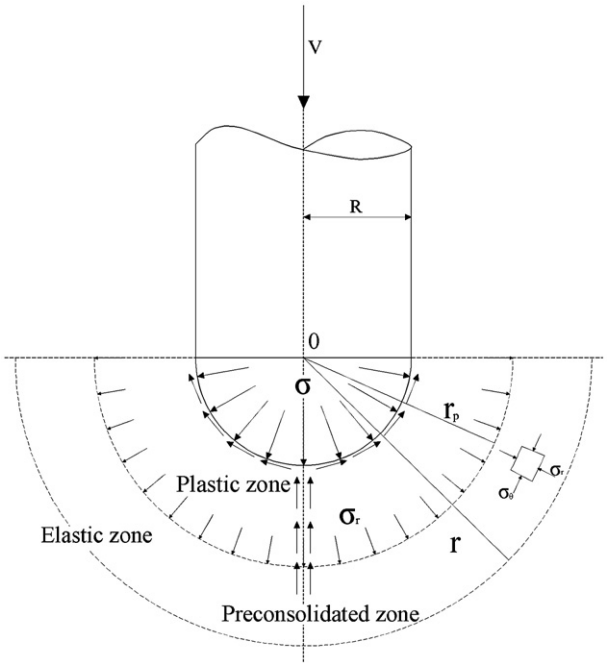

Fig. 2. Spherical cavity expansion.

so that the internal pressure of concrete will also increase from 0 to $\sigma(t)$. Concrete around the expansion cavity will become deformed, plasticizing if the applied pressure is higher enough. This spherical volume, plasticized around the cavity, has a radius (r_p) and will push the paste around in an elastic equilibrium state, defined by Young's and Poisson's moduli, causing its consolidation, which will be less when farther from the penetrator surface.

The stresses around the sphere will be similar to those produced around a conical penetrator, defined by Su and Liao [22]. Beneath the sphere, the mass will be subjected to axial compression, with its major principal stress in the vertical direction (σ_1) and the minor principal stress (σ_3) in the horizontal direction. For concrete around the spherical surface, the stress state is close to that of a cavity that expands, with the major principal stress normal to the penetrator surface, and the minor principal stress, tangential to this. The area located around the vertical wall of the crater also has major stresses similar to those of a cavity that expands, with the mayor principal stress rotating from the vertical to the horizontal direction.

When the sphere impacts on fresh concrete, it penetrates at initial speed (v_0) which becomes progressively reduced until it stops [23] (Fig. 3). During the first penetration moments, a great volume of concrete around the sphere gets plasticized, but due to the sphere movement, the concrete volume that previously was compressed gets decompressed, being pre-consolidated, and the zones that were plasticized get irreversibly deformed by the sphere movement [24]. Progressively the penetration speed diminishes, so that the plastification spheres, as well as the pre-consolidated volume becomes smaller, until the projectile movement stops and if the depth of penetration is bigger than the sphere radius, the plasticized volume radius is equal to the sphere radius.

So, concrete behavior beneath the sphere when it is stopped is elastic. As concrete is an isotropic material, the relation between the stress increment applied and the deformation increment produced will be given by Hooke's law:

$$d\varepsilon_{11} = \frac{1}{E} d\sigma_{11} - 2\frac{v}{E} d\sigma_{22}. \tag{3}$$

And as in fresh concrete, before the setting time, pressures are hydrostatic [25], considering effective stresses in the horizontal direction ($d\sigma_{22}$) approximately equal to zero, it can be said that:

$$d\varepsilon_{11} = \frac{1}{E} d\sigma_{11}. \tag{4}$$

2.3. Materials

As this paper is framed within an investigation about concrete pavements, the total aggregate distribution dosage used

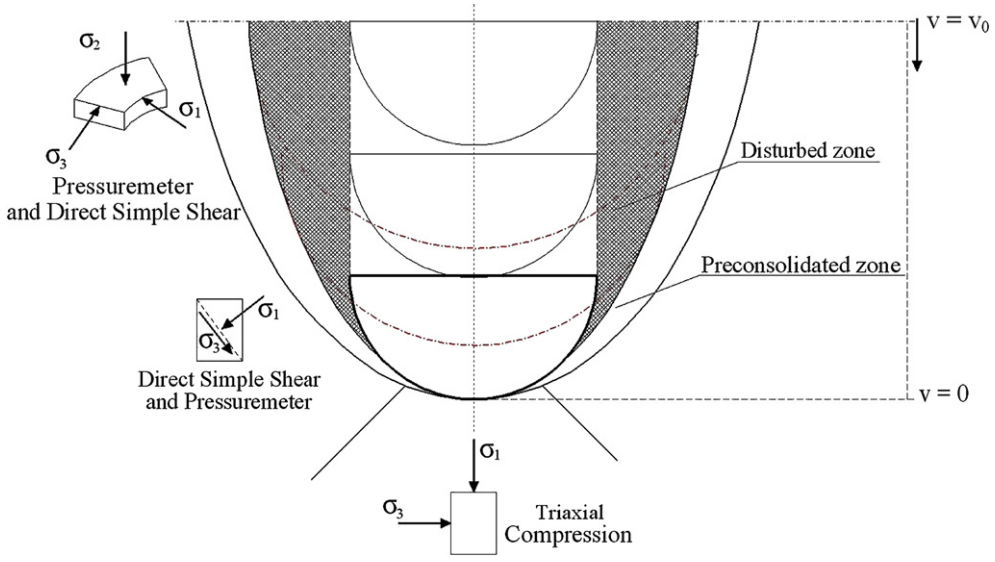

Fig. 3. Failure modes around the sphere.

has been designed by, (i) the percent aggregate retained method (Fig. 4(a)), so that the total combined aggregate particles have a tolerance of acceptable size distribution, and by (ii) the combined aggregate distribution (Fig. 4(b)), with the purpose of obtaining an appropriate mixture for the manual placement of concrete [26]. The aggregate distribution dosage is given in Table 1.

Four types of cement were used in the tests (CEM I 52.5R (UNE EN 197-1), CEM II/A-V 42.5 R (UNE EN 197-1), CEM IV/A (V) 32.5 N/SR (UNE EN 80 303-1)). In order to know the temperature influence in the setting time for each one of these cements, their activation energy was studied in a similar way to that used by Pinto and Hover [27], obtaining the results given in Table 2.

Forty-five different dosages were made in which the total aggregate distribution was maintained, varying the type and quantity of cement and the water–cement ratio (it has been demonstrated that non-reactive aggregates do not influence the total setting time [25]).

Finally, to have an idea of the validity of the model, three real pavements were studied, each of them with the aggregate distribution dosage given in Table 1, although as will be explained, this is not important for the model validation. The water to cement ratio, as provided by the constructor, was 0.49.

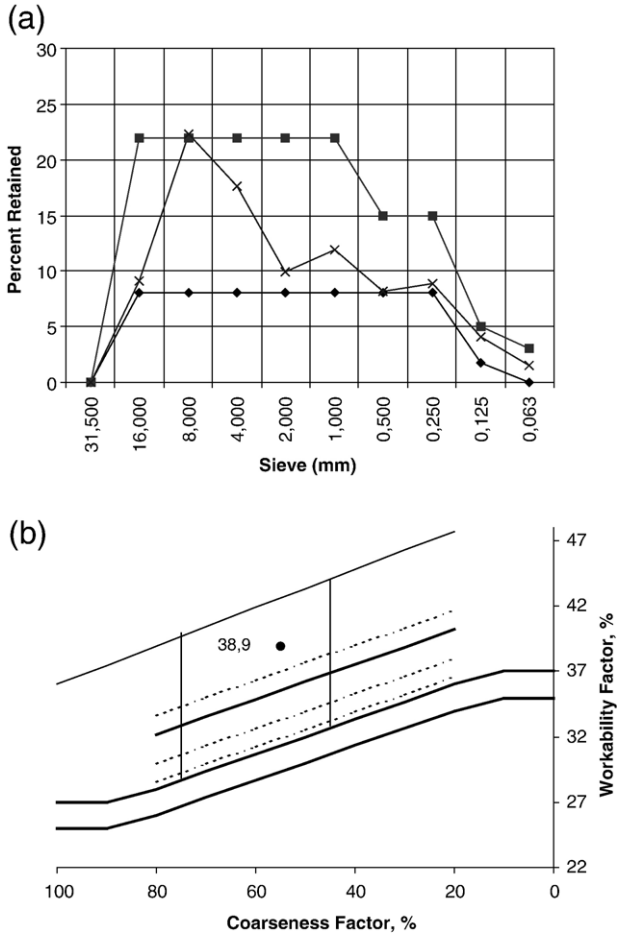

Fig. 4. Combined aggregate gradings: (a) Percentage of the combined aggregate retained in each sieve; (b) workability factor of the aggregates.

Table 1
Combined aggregate distribution, %

Type of material	Percentages (%)
Limestone sand	12
Silica sand	36
Gravel, 4–12 mm	28
Gravel, 12–32 mm	24

2.4. Test procedures

Each of the forty-five dosages was tested three times in molds such us the one in Fig. 1, so that each penetration resistance–time curve (Fig. 8) had at least fifty points. The mix was carried out in a vertical axis concrete mixer for at least 3 min. Later an Abrams cone test was done for the mold as described in UNE 83-313-90 [28], the concrete was poured into the molds, extended, and uniformly vibrated with a 35 mm and 6000 rpm vibrator and finally, the surface was flattened.

For the three real pavements studied, the tests were conducted with the same concrete used in the pavement and in the same ambient conditions.

All concrete was made at ambient temperature, during a period of time from July until December, 2005 in which temperatures oscillated from 26 °C to 8 °C and the ambient humidity from 83% to 56%.

3. Formulation of the model

3.1. Stress-deformation states in concrete

According to the Terzaghi principle [28], the stress at any point of a soil mass can be studied through the total principal stresses which act in it. Concrete, as a soil, is a three-phase system and if its holes are filled with water, when applying a load to the mass (σ), it will be equally distributed between the mineral skeleton and the interstitial fluid. So effective stresses that deform the floor or the concrete are the excess ones over the hydraulic pressure (u) in the mass: $\sigma' = \sigma - u$. In the case of a cementitious material p and u have a very similar value, so the effective stresses in the material at rest tend to be null [25,30].

It was also important to consider for the model the relationship between the depths reached by the penetrator in time and the specific volume of concrete (v). For this, the hypothesis that the variation of specific volume in time (dv/dt) is equal but with an opposite sign to the variation of depth in time (dy/dt) was made:

$$\frac{dy}{dt} = -\frac{dv}{dt}. \tag{5}$$

With reference to the variations of specific volume at early ages, they happen because in the very early stages after mixing the cement with water, the hydration products require a smaller volume than the individual compounds. This is called chemical shrinkage. Otherwise, it also depends on the surface tension of the pore solution and the meniscus radius of the largest water-filled pores within the microstructure [31], variable with time

Table 2
Activation energy until the initial setting time (kJ/mol)

CEM I 52.5 R (UNE-EN 197-1)	32.24
CEM II/A-V 42.5R (UNE-EN 197-1)	26.46
CEM II/B-M (V-LL) 32.5 (UNE-EN 197-1)	26.73
CEM IV/A 32.5 N/SR (UNE 80 303-1)	28.49

due to water adsorption by cement, so that when the mass acquires enough resistances to sustain itself, it operates as a passive internal restraint system that resists deformations and reduces the physical shrinkage. Sometimes it is also due to the external forces applied, such us a footprint in fresh concrete:

$$dv = dv_p + dv_s \tag{6}$$

where:

v_p Variation of specific volume due to the external forces applied.
v_s Variation of specific volume due to the process of concrete cementation.

In the case of concrete, deformations due to the cementation process are always irrecoverable: although this process can increase or diminish its speed, its effects cannot be reverted, while the deformations due to external agents may be both recoverable and irrecoverable. For a given time, if deformations made by a sphere falling from different heights are plotted against the stress logarithm made by that sphere, a straight line is obtained (Fig. 5) which can be related to the Cam clay model equations [29]:

$$d\varepsilon_v^p = \frac{dv}{v} = \frac{\lambda(t)}{v}\cdot\frac{dp'}{p'} \tag{7}$$

$$d\varepsilon_v^e = \frac{dv}{v} = \frac{k(t)}{v}\cdot\frac{dp'}{p'} \tag{8}$$

where p' is the hydrostatic stress, $\lambda(t)$ and $k(t)$ are the stiffness parameters or the slopes of the lines which relate stress to the specific volume variation and correspond, respectively, to the plastic and elastic lines; that is to say, they represent the concrete stiffness. They are constant at an instant, but growing in time, due to the increase of concrete stiffness with time.

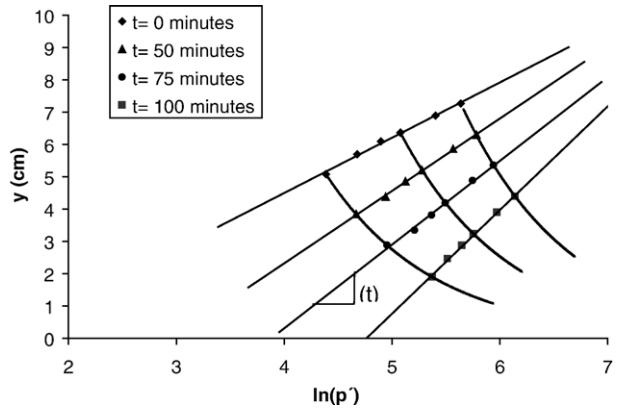

Fig. 5. Fresh concrete $y-\ln(p')$ curve with time.

From the integration of Eqs. (7) and (8) as a function of p', the following will be obtained:

$$v_1 = v(t) - \lambda(t)\cdot\ln p' \text{ (Plastic lines)} \tag{9}$$

$$v_1 = v(t) - k(t)\cdot\ln p' \text{ (Elastic lines).} \tag{10}$$

These equations are valid only in a certain range, because although p' is increased to infinite, v cannot be indefinitely reduced, since a maximum of collapse at a given instant will always exist.

One example of this is the vibration of concrete, which can be supposed equivalent to soil consolidation (Fig. 6): a stress is applied with the vibrator that causes deformations from V_a until a maximum V_b. In this situation, concrete moves along a plastic line (Line a–b), and it will not return to the previous deformation state after removing the vibrator (Line b–c). As the mass acquires resistances, the penetrator will move by a series of instantaneous elastic lines until the time when the penetration resistance is higher than the stress that the concrete has suffered during the vibration process, from that point, the sphere will move by a series of plastic lines.

Bearing in mind that when the sphere falls, before the setting time, the stresses are equally distributed between the solid skeleton and water [25–29] and as deformations are the same for both phases, the total stiffness variation in the mass will be:

$$\frac{d\lambda(t)}{dt} = \frac{1}{2}\cdot\frac{d\lambda(t)_{tc}}{dt} + \frac{1}{2}\cdot\frac{d\lambda(t)_c}{dt} \tag{11}$$

where:

$\frac{d\lambda(t)}{dt}$ Total stiffness variation in the mass of concrete
$\frac{d\lambda(t)_{tc}}{dt}$ Stiffness variation due to the capillary stress
$\frac{d\lambda(t)_c}{dt}$ Stiffness variation due to the cementation process.

With regard to the stiffness caused by the cementation process, numerous investigations show that there is a relationship between the compressive strength, the heat produced and the hydration degree [13,32]. When representing this on a logarithmic scale it is

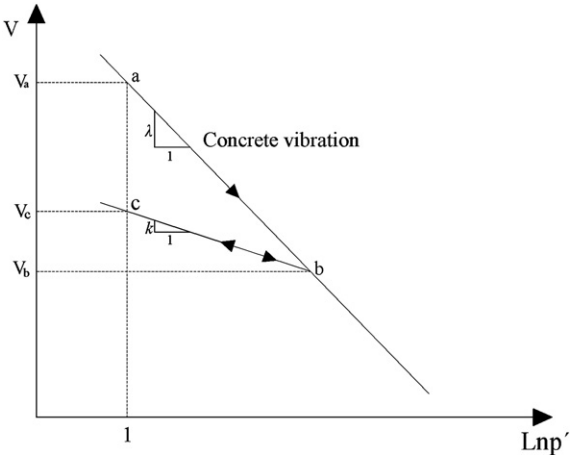

Fig. 6. Proposed stress-deformation behavior of concrete during the vibration process, supposing it to be instantaneous.

found that this is non-linear at the start of hydration, but later it becomes so. Studies performed by Byfors [13], show an initial distance without resistance, followed by a non-linear small section and later another linear one. In his own words: "…the relation between strength and the degree of hydration is, however, exponential at a very early stage, from the setting phase and to few hours after". This exponential behavior is also explained in the ASTM C 403 [33].

On the other hand, as a loss of free water among particles takes place in concrete at a certain speed due to the water adsorption of cement, it will be possible to compare the material stiffness variation due to the capillary stress with the behavior of a non-saturated soil, in which suction affects its mechanical behavior. One of the most popular models which predict this situation is the BBM (Barcelona Basic Model) [34]. An elastoplastic model, able to reproduce the stress-deformation behavior of non-saturated soils, supposing they do not show anisotropy or expansivity. The equation which describes the plastic stiffness increase in a soil with suction is:

$$\lambda(s) = \lambda(0) \cdot ((1 - r) \cdot \exp(-\beta \cdot s) + r) \tag{12}$$

where $\lambda(s)$ is assumed to vary exponentially from $\lambda(0)$, which is the initial soil stiffness at zero suction, to $r \times \lambda(0)$ which is the stiffness as suction tends to infinity. The rate of stiffness increase with suction is controlled by the parameter β.

3.2. Deformations in fresh concrete

Talking about concrete, it is difficult to believe in an asymptote when time tends to infinity due to the stiffness variation by suction. This is because during strength acquisition there is a time when the mass is not a granular material any more, becoming a solid (setting time). However, at least until the setting of concrete, the stiffness due to water adsorption by the cement can be supposed to decrease exponentially. So, noting that r is zero and that in concrete suction must be substituted by time, from Eq. (12), it can be assumed:

$$\frac{d\lambda(t)_{tc}}{dt} = -\beta \cdot \lambda(0) \cdot \exp(-\beta \cdot t) \tag{13}$$

where $\lambda(0)$ is the initial concrete stiffness at time zero and β is the average rate of stiffness increase with time.

If losses of free water from the setting process such us evaporation are not considered, it can be assumed that the speed at which free water disappears, is the same as its adsorption rate by the cementitious materials. So, knowing that initial stiffness $\lambda(0)$ will be equal for both processes, that β is the average speed at which the hydration process occurs and that the stiffness evolution in time will be exponential during the first hours [13], it can be made the hypothesis of exponential stiffness variation due to the cementation process:

$$\frac{d\lambda(t)_c}{dt} = \beta \cdot \lambda(0) \cdot \exp(\beta \cdot t). \tag{14}$$

So, the total stiffness variation in the mass of concrete will be:

$$\frac{d\lambda(t)}{dt} \beta \cdot \lambda(0) \cdot \left(\frac{\exp(\beta \cdot t) - \exp(-\beta \cdot t)}{2}\right) \tag{15}$$

which simplified:

$$\frac{d\lambda(t)}{dt} = -\beta \cdot \lambda(0) \cdot \sinh(\beta \cdot t) \tag{16}$$

Then, during the first hydration hours, stiffness variation can be understood as an hyperbolic sine and the stiffness at a given time during the first hydration hours will be given by:

$$\lambda(t) = \lambda(0) \cdot \cosh(\beta \cdot t) \tag{17}$$

which is the slope, variable with time, of the straight lines in Fig. 5. Nevertheless, the desired relationship is the one between the concrete deformation and the penetration resistances increment in time, not instantaneously ($K(t)$) (Fig. 11), which is the same as normal curves to the straight lines with slope $\lambda(t)$ in Fig. 5:

$$(\lambda(t))^{-1} = K(t) = \frac{1}{\lambda(0)} \cdot \operatorname{sech}(\beta \cdot t). \tag{18}$$

On the other hand, the relative deformations will be:

$$\varepsilon(t) = \frac{y(t)}{y(0)}, \text{ with } \varepsilon(0) = 1. \tag{19}$$

As demonstrated by Chen and Li [20], the final penetration depth in an impact has no dependence on the geometry function of the projectile, so a way to simplify the calculation without influencing the final result will be to substitute the volume displaced by the sphere for a cylinder in Eq. (2), so that taking Eq. (19) into account, stresses at each moment are:

$$\sigma(t) = \frac{m \cdot g \cdot H}{A \cdot \varepsilon(t) \cdot y(0)} \tag{20}$$

where A is the area of the spherical portion in contact with concrete projected in the horizontal plane.

Relating Eqs. (4) and (7) with Eq. (2), taking into account that $\lambda(t)$ must be substituted by $K(t)$ and simplifying the concrete volume displaced by the penetrator as if it were a cylinder the relationship between the elastic modulus of concrete and its stiffness can be obtained:

$$E(t) \frac{m \cdot g \cdot H}{A \cdot K(t)}. \tag{21}$$

Substituting Eqs. (20) and (21) into Eq. (4):

$$\sigma(t) = E(t) \cdot \varepsilon(t) \rightarrow \frac{m \cdot g \cdot H}{A \cdot \varepsilon(t) \cdot y(0)} = \frac{m \cdot g \cdot H}{A \cdot K(t)} \cdot \varepsilon(t) \tag{22}$$

and simplifying $\varepsilon(t)$:

$$\varepsilon(t) = \sqrt{\frac{K(t)}{y(0)}}. \tag{23}$$

Besides, Eq. (23) at time zero:

$$(\lambda(0))^{-1} = K(0) = y(0). \tag{24}$$

And relating Eq. (18) with Eqs. (23) and (24), the relative volumetric deformation in the mass due to the impact is obtained, which varies with time:

$$\varepsilon(t) = \sqrt{\operatorname{sech}(\beta \cdot t)}. \tag{25}$$

So, from Eq. (25) the conclusion can be drawn that relative deformations in concrete are unrelated to the impact energy or the geometry of projectile, only depending on those factors that make hydration kinetics vary.

This equation predicts a decrease in the relative deformations of concrete with time by an object falling, tending to zero when time tends to infinity $\lim_{t\to\infty}\varepsilon(t) = 0$, which means an unlimited increase of stiffness. So, this equation would only be valid in a short period, from the concrete placement until a given instant. With the purpose of avoiding this situation, it has been assumed that when time tends to infinity, the relative deformations tend to a certain value $(r)\lim_{t\to\infty}\varepsilon(t) = r = y(\infty)/y(0)$. So Eq. (25) becomes:

$$\varepsilon(t) = (1-r)\cdot\sqrt{\operatorname{sech}(\beta \cdot t)} + r. \tag{26}$$

In Fig. 7, Eq. (26) is shown in a graph with time represented on a logarithmic scale, where a similarity with the consolidation curves for soils represented by the logarithmic method can be observed [28]. It consists of three parts: an initial one with approximately parabolic shape, a linear section and a final curve with a horizontal asymptote at $r \approx 0$. From these curves it is important to point out two characteristic points (A and B in Fig. 7). In the first place A, which corresponds to the maximum consolidation reached by concrete during the vibration process. Secondly point B, whose most probable value of relative deformation according to the experimentally obtained results from the forty-five samples is 0.18 (Fig. 8). In this case, after applying Chauvenet's criteria to the data Pearson's correlation coefficient is approximately 0.98 with p-value exceeding 0.25. The normal probability plot for the standard normal distribution is almost linear, which indicates agreement with the normality assumption.

The decrease of depths from concrete vibration to point B is similar to the concept of primary deformation, used in geotechnics, in which free water still exists in the pores and therefore there are overpressures when applying a stress in the mass. From point B, the curve is similar to the concept of secondary consolidation, in which the mineral skeleton acquires different properties of stress-deformation to those it had previously: the mass begins to behave as a solid and the loads are no longer distributed equally between the liquid and the solid.

The value B of relative deformation 0.18 is very similar to the value 0.16 in the universal percolation threshold and is very reasonable to think that this instant corresponds with the value 0.18 of capillary porosity in the percolation threshold reported by Garbocci and Bentz [4], with the 20% porosity described by Powers et al. [35] when the capillary pores in cement paste exhibit a percolation transition from connected to disconnected, as well as with the time at which the hydrostatic pressure of concrete becomes zero [25]. So this moment will probably be the initial setting time, but further investigation is required.

Finally, recalling Eq. (19) and substituting it into Eq. (26), the evolution of the penetration depth in fresh concrete for impacts with the same penetrator and energy will be as follows:

$$y(t) = y(0)\cdot[(1-r)\cdot\sqrt{\operatorname{sech}(\beta \cdot t)} + r] \tag{27}$$

where it is shown that the total depth of penetration in concrete at a given time is function of the initial depth of the crater, the

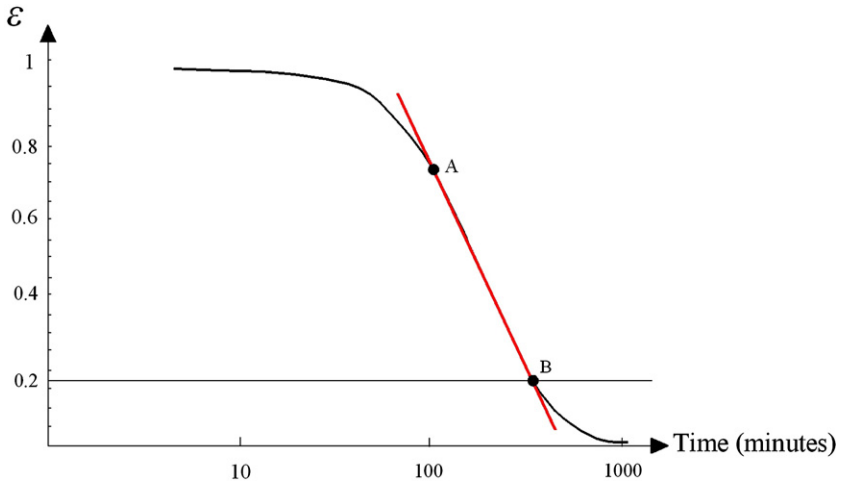

Fig. 7. Relative depth of the crater–log(time) curve.

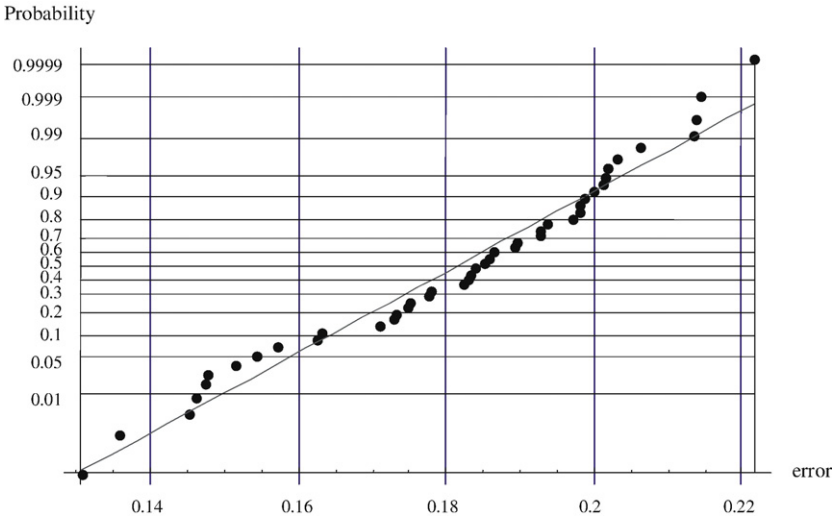

Fig. 8. Point B represented in normal probability plot for all the samples made.

hydration kinetics and the ultimate strength resistance of concrete represented by *r*.

4. Results, discussion and model validation

As Fig. 9 shows, a good correlation exists between the theoretical model and the experimental data obtained during the period of study. This example is for a concrete made with 444 kg/m^3 of CEM II/A-V 42.5R and a water–cement ratio of 0.52. Its slump by the method of the Abrams cone test was 3, the ambient humidity was 58% and the average temperature in the mass was 19.1 °C. After applying Chauvenet's criteria to the data, Pearson's correlation coefficient in this case is 0.997 and the 95% confidence interval for the penetration depth error was of 9%. In the case of the samples analyzed, the correlation coefficient was always better than 0.992. Moreover, for all the craters studied, there is a probability that 95% have a confidence interval for the penetration depth better than 18%. One of the best proof of the validation of a model is the normality of its errors, in this case, in Fig. 10 the distribution of the error percentage is represented with regard to the model in a normal probability plot. Here, Pearson's correlation coefficient is 0.996 and the *p*-value exceeds 0.25. As expected, the normal probability plot is almost linear, which confirms the hypothesis of normality. In no sample was the distribution of errors not normal.

There are different maturity functions to determine the strengths variation and the degree of hydration of concrete with time. The two models commonly used are the linear hyperbolic and parabolic hyperbolic models, both developed by Knudsen [36,37]; the difference between them is described in terms of

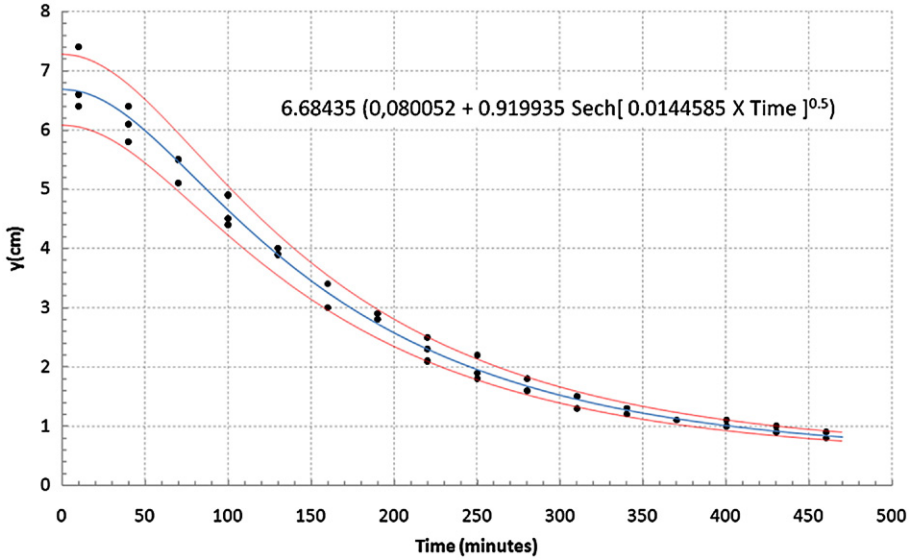

Fig. 9. Depth of the crater–time curve with its confidence intervals.

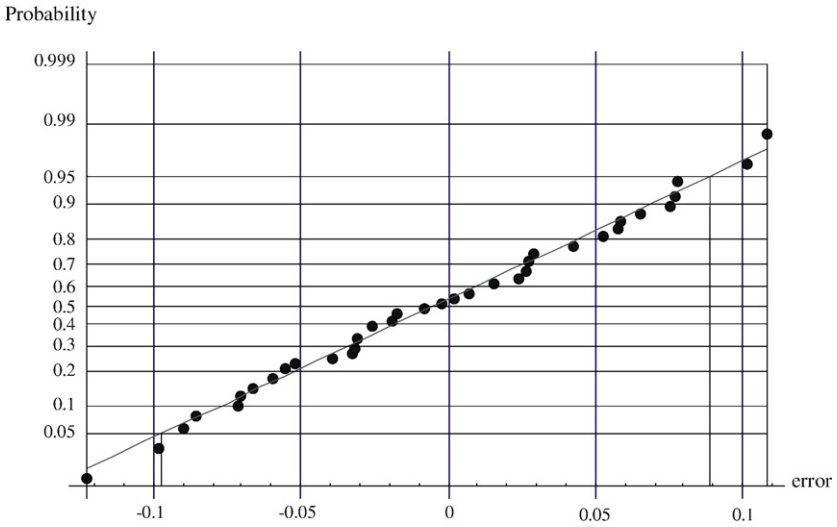

Fig. 10. Normal probability plot of errors.

hydration kinetics of the cement particles. The linear dispersion model, represented in Eq. (28), considers the hydration degree of an individual cement particle as a linear function of the product of time and a constant β which represents the hydration kinetics [38]; in this model, t_0 is the age at the start of strength development and S_u is the asymptotic value of limiting strength.

$$S = S_u \cdot \frac{\beta \cdot (t - t_0)}{1 + \beta \cdot (t - t_0)}. \tag{28}$$

The parabolic model, as shown in Eq. (29), considers that the hydration degree is a function of the square root of the product of time and a constant [37]. According to Bentz [30], Eq. (29) provides a better adjustment with regard to the experimental data. This equation is not valid for early hydration ages ($0<\alpha<0.15$), but it is well suited for modeling when $\alpha>0.15$ [37]; although, Bentz [39] suggested that Eq. (29) could be capable of modeling for values over the hydration degree $\alpha>0.1$

$$S = S_u \cdot \frac{\sqrt{\beta \cdot (t - t_0)}}{1 + \sqrt{\beta \cdot (t - t_0)}}. \tag{29}$$

An expression of the penetration resistance of fresh concrete with the variables taken into account in this paper may be found by simply substituting Eq. (20) into Eq. (27), so that if the previously mentioned hypotheses are correct, the results obtained are

$$\sigma(t) = \sigma(0) \cdot \frac{\sqrt{\cosh(\beta \cdot t)}}{(1 - r) + r \cdot \sqrt{\cosh(\beta \cdot t)}}. \tag{30}$$

It can be seen that Eq. (30) is quite similar to Eq. (29), with the exception that this is not a good model for small hydration

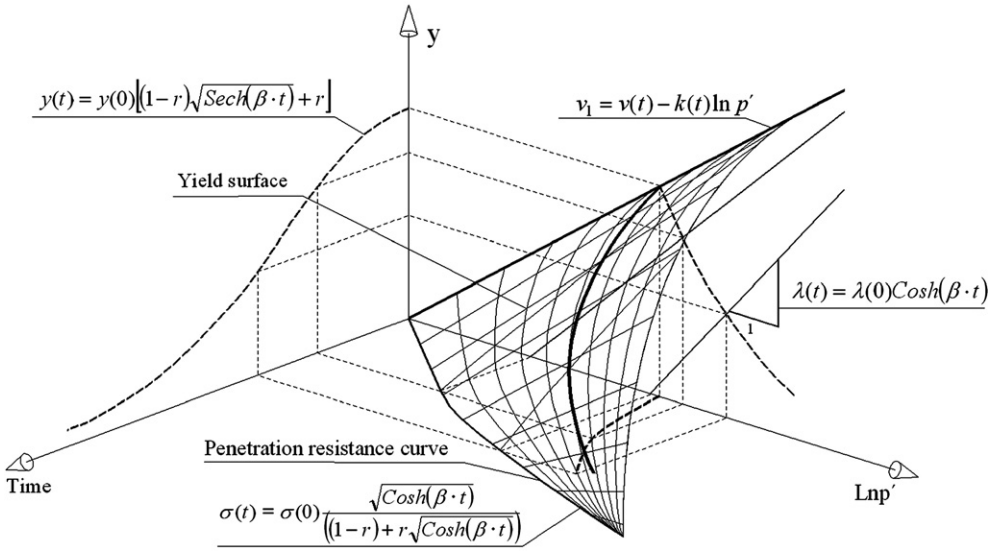

Fig. 11. Yield surface of fresh concrete during the first hours of hydration.

degrees, while Eq. (30) has been deduced for these. Besides, the proposed equation is S shaped, being the maximum produced in hydration kinetics through time reflected [13].

Finally, as when time tends to infinity, r is approximately zero ($r=\sigma(0)/\sigma(\infty)\approx 0$), Eq. (30) can be approximated by the following at very early ages, counting time from the moment when the cement is mixed with water:

$$\sigma(t) = \sigma(0) \cdot \sqrt{\cosh(\beta \cdot t)}. \quad (31)$$

ASTM C403 [33] shows how the penetration resistance of concrete at early ages can be approximated by means of a potential equation. However, this solution supposes the penetration resistances at time zero to be null, forgetting that it can be useful to know this period, for example, in the case of a concrete pavement, which is the most extended use for the Proctor needles, the time of starting trowelling. Then, the use of Eq. (26) is proposed as a more rational approach to find out the evolution of penetration resistances with time than the equation given by ASTM C403.

Finally, Fig. 11 shows a three-dimensional view of the yield surfaces in (t, y, p) stress space, where the depth of penetration (y) of the sphere in time is the projection of the curve normal to the straight line stress-deformation on the yield surface of fresh concrete. The shear line of this surface with the stress-time plane coincides with the resistance curve to penetration defined in ASTM C403, and the slope of the shear line of the yield surface with the stress-penetration plane is an indicator of the initial consistency of concrete; a variation of this parameter, due to any cause, such as a change in concrete temperature, ambient humidity or water/cement ratio, will be reflected in the depths of the craters, so that the slopes of the penetration–time curves will be increased or diminished. In the case of a change of hydration kinetics in concrete, a displacement will occur in the penetration resistance curve in the mass, as well as a variation in the speed of change in the concrete stiffness, with which the slopes of the penetration–time curve will be increased or diminished, too.

5. Practical application

In this paper, we point out that one of the main applications of this model is to know the initial setting time. We postulate that this time coincides with the time to start power floating a concrete pavement. Traditionally, workers have intuitively chosen this time. ACI 302.1R-96 [40], advises to wait for the finishing operations "until the concrete will sustain foot pressure with only about 6 mm indentation". Otherwise, the time indicated by ASTM C403 as the setting time, is sometimes also considered the time to start the finishing operations in a concrete pavement.

Table 3
Results of three samples for the practical application of the model

	Sample 1	Sample 2	Sample 3
$y(0)$ (cm)	17.1	11.8	19.4
Theoretical depth ($0.17y(0)$) (cm)	2.9	2.1	3.9
Depth penetration in the time chosen by the workers for the finishing operations (cm)	2.7	2.3	3.3
Theoretical time of initial setting of concrete (min)	117	233	85
Time chosen by the workers for the finishing operations (min)	117	226	95

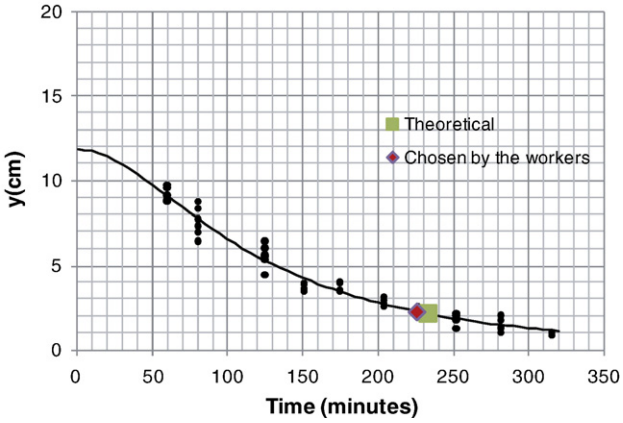

Fig. 12. Depth of the crater–time curve for a real pavement.

To have an idea of the applicability of the model, three different real pavements were studied. From these tests, the results are shown in Table 3. For the three samples studied, the maximum difference between the theoretical time to start trowelling the concrete pavement (when $y(t)=0.18\times y(0)$ in Eq. (27)) and the time chosen by the workers to start this process was 10 min, although the initial consistence for the three real concretes studied was different so as the ambient conditions, which is a proof of how the model provides a level of accuracy that has not been seen before. Although three tests are not enough for the on site validation of the model, they give a very good idea about how to use this level of accuracy for the timming of construction operations. In Fig. 12, the depth of the crater–time curve for the Sample 2 is shown. From this figure, it can be appreciated how the proposed model fits very well to the data and how the theoretical time to start trowelling a concrete pavement, being zero the placement time, almost coincide with the real time when the workers, intuitively, started trowelling the concrete. Finally, it is interesting to point that the third sample was made during the summer, in the street, with more than 30 °C temperature and a wind of approximately 15 km/h; in this situation, the results were not worse than in the others, and the theoretical time of initial setting almost coincided with the time that the workers chose for the finishing opperations. In any case, more research is required about the practical applications of this method.

6. Conclusions

In this paper a new concept has been applied for the initial setting of concrete, different to those which are traditionally used. For that, a semiempirical model has been developed that physically explains the processes that occur until the initial setting of concrete. Among the advantages of the proposed method are: a better explanation of the strength acquisition of concrete during this period, an excellent approximation, and

even the facility of predicting the initial setting time at very early ages by means of an extrapolation of the predicted curves.

Behavior of fresh concrete when hardening is comparable to soil consolidation as defined by the log time method, thus the secondary consolidation of concrete takes place when the depth of the crater made by a falling object is 18% of the initial depth. This value is very similar to the universal percolation threshold, independently of the speed, mass or geometry of the penetrator and depending only on the hydration kinetics of concrete. It is proposed that it corresponds with the initial setting of concrete although further investigation is required.

Sometimes, penetration resistance setting data, as indicated in ASTM C403, can be the cause of serious errors, such us as when they are compared with the Vicat ones, because these are always made with the same "normal consistency". Therefore, in this paper a change in the concept of initial setting as explained in the ASTM C403 is proposed because as has been explained, the value for the initial setting time does not depend on the penetration resistance of concrete but on its percolation degree.

References

[1] L. Struble, K. Yong, T. Zhang, Setting of cement and concrete, Cem., Concr., Aggreg. 23 (2) (2001) 88–93.

[2] Z. Sun, T. Voigt, S. Shah, Edometric and ultrasonic viscoelastic properties of fresh Portland cement pastes, Cem. Concr. Res. 36 (11) (2006) 278–287.

[3] L. Zhuguo, T. Onkubo, Y. Tanigawa, Flow performance of high-fluidity concrete, J. Mater. Civ. Eng. 16 (6) (2004) 558–596.

[4] E.J. Garbocci, D.P. Bentz, The microstructure of Portland cement-based materials: computer simulation and percolation theory, Mat. Res. Soc. Symp. Proc. 529 (1998) 89–100.

[5] J.M. Hammersley, Percolation processes II. The connective constant, Proc. Camb. Philos. Soc. 53 (1957) 643–645.

[6] R. Zallen, The Physics of Amorphous Solids, J. Wiley and Sons, New York, 1983.

[7] H. Scher, R. Zallen, Critical density in percolation processes, J. Chem. Phys. 53 (9) (1970) 3759–3761.

[8] UNE-EN 196-3, Método de ensayo de cementos. Parte 3: Determinación del tiempo de fraguado y estabilidad de volumen, 1996.

[9] Nordtest Method NT BUILD 476 Fresh Concrete: Initial Setting Time and Activation Energy During Setting.

[10] L.H. Tuthill, W.A. Cordon, Properties and uses of initially retarded concrete, Proc. - Am. Concr. Inst. 52 (2) (1955) 273–286.

[11] ASTM C 403/C 403M-99, Standard Test Method for Time of Setting of Concrete Mixtures by Penetration Resistance.

[12] A.K. Schindler, Prediction of concrete setting, RILEM International Symposium on "Advances in Concrete Through Science and Engineering", Evanston, Illinois, March 22–24 2004.

[13] J. Byfors, Plain concrete at early ages, Technical Report, Swedish Cement and Concrete Research Institute, S-100 44 Stockholm, 1980.

[14] I. Albert, P. Tegzes, R. Albert, J.G. Sample, A-L. Barabási, T. Vicsek, B. Kahng, P. Schiffer, Stick-slip fluctuations in granular drag, Phys. Rev. E (2001) 031307.

[15] R. Albert, M.A. Pfeifer, A.L. Barabási, P. Schiffer, Slow drag in a granular medium, Phys. Rev. Lett. 82 (1999) 205–208.

[16] J.R.C. Garry, M.C. Towner, A.J. Ball, J.C. Zarnecki, G. Marcou, The effect of ambient pressure on low speed penetration of unconsolidated materials, Adv. Space Res. 23 (7) (1999) 1229–1237.

[17] J.E. Herrick, T.L. Jones, A dynamic cone penetrometer for measuring soil penetration resistance, Soil Sci. Soc. Am. 66 (2002) 1320–1324.

[18] J.S. Uehara, M.A. Ambroso, R.P. Ojha, D.J. Duran, Low-speed craters in loose granular media, Phys. Rev. Lett. 90 (19) (2003) 194301.

[19] J.R. de Bruyn, A.M. Walsh, Penetration of spheres into loose granular media, Can. J. Phys. 82 (2004) 439–446.

[20] X.W. Chen, Q.M. Li, Deep penetration of a non deformable projectile with different geometrical characteristics, Int. J. Impact Eng. 27 (2002) 619–637.

[21] D. Markauskas, R. Kacianauskas, M. Suksta, Modelling the Cone Penetration Test by the Finite Element Method, Publishing House of Poznan Universty of Technology, 2002.

[22] S.F. Su, H.J. Liao, Influence of strength anisotropy on piezocone resistance in clay, J. Geotech. Geoenviron. Eng. 128 (2) (2002) 166–173.

[23] W.A. Allen, E.B. Mayfield, H.L. Morrison, Dynamics of a projectile penetrating sand, J. Appl. Phys. 28 (1957) 370–376.

[24] J.A. Jiménez Salas, J.L. de Justo Alpañes, A. Serrano González, Geotecnia y Cimientos, Mecánica del Suelo y de las Rocas, vol. II, Editorial Rueda, (Madrid), 1976.

[25] S. Amziane, Setting time determination of cementitious materials based on measurements of the hydraulic pressure variations, Cem. Concr. Res. 36 (2006) 295–304.

[26] P.J. Harrison, For the ideal slab on ground mixture, ACI Concr. Int. 26 (3) (2004) 49–55.

[27] R.C.A. Pinto, K.C. Hover, Application of maturity approach to setting times, ACI Mat. J. 96 (6) (1999) 686–691.

[28] UNE 83-313-90, Ensayos de hormigón. Medida de la consistencia del hormigón fresco. Método del cono de Abrams.

[29] J.A. Jiménez Salas, Geotecnia y Cimientos, Propiedades de los Suelos y de las Rocas, vol. I, Editorial Rueda, (Madrid), 1975.

[30] J. Asaad, K.H. Khayat, Variations of lateral and pore water pressure of self-consolidating concrete at early age, ACI Mat. J. 104 (4) (2004) 310–317.

[31] D.P. Bentz, A three dimensional cement hydration and microstructure program I. Hydration rate, Heat of Hydration and Chemical Shrinkage, NISTIR No. 5756, U.S. Department of Commerce, Washington, D. C., Nov. 1995.

[32] J.H. Taplin, A method for following the hydration reaction in Portland cement paste, J. H. Aust. J. Appl. Sc. 10 (1959) 329–345.

[33] ASTM C 403/C 403M-99, Standard Test Method for Time of Setting of Concrete Mixtures by Penetration Resistance.

[34] E.E. Alonso, A. Gens, A. Josa, A constitutive model for partially saturated soils, Géotechnique 40 (3) (1990) 405–430.

[35] T.C. Powers, L.E. Copeland, H.M. Mann, Capillary continuity or discontinuity in cement pastes, PCA Bull. 1 (110) (1959) 2–12.

[36] T. Knudsen, On Particle Size Distribution in Cement Hydration, Proc. of the 7th Intl. Congr. on the Chem. of Cement, Paris, vol. II, 1980, pp. I–170–175.

[37] T. Knudsen, Dispersion model for hydration of Portland cement: I. General concepts, Cem. Concr. Res. 14 (1984) 622–630.

[38] N.J. Carino, The maturity method: theory and application, Cem., Concr., Aggreg. 6 (2) (1984) 61–73.

[39] D.P. Bentz, Three-dimensional computer simulation of Portland cement hydration and microstructure development, J. Am. Ceram. Soc. 80 (1) (1997) 3–21.

[40] ACI Committee 302, Guide for Concrete Floor and Slab Construction, ACI 302.1R-96, American Concrete Institute, Farmington Hills, Michigan, 1996.